Emerald Insight

Sensor Review

A double-end-beam based infrared device fabricated using CMOS-MEMS process

Cheng Lei Haiyang Mao Yudong Yang Wen Ou Chenyang Xue Zong Yao Anjie Ming Weibing Wang Ling Wang Jiandong Hu Jijun Xiong

Article information:

To cite this document:
Cheng Lei Haiyang Mao Yudong Yang Wen Ou Chenyang Xue Zong Yao Anjie Ming Weibing Wang Ling Wang Jiandong Hu Jijun Xiong , (2016),"A double-end-beam based infrared device fabricated using CMOS-MEMS process", Sensor Review, Vol. 36 Iss 3 pp. -
Permanent link to this document:
http://dx.doi.org/10.1108/SR-02-2016-0038

Downloaded on: 30 June 2016, At: 01:30 (PT)
References: this document contains references to 0 other documents.
To copy this document: permissions@emeraldinsight.com
The fulltext of this document has been downloaded 9 times since 2016*

Access to this document was granted through an Emerald subscription provided by emerald-srm:393177 []

For Authors

If you would like to write for this, or any other Emerald publication, then please use our Emerald for Authors service information about how to choose which publication to write for and submission guidelines are available for all. Please visit www.emeraldinsight.com/authors for more information.

About Emerald www.emeraldinsight.com

Emerald is a global publisher linking research and practice to the benefit of society. The company manages a portfolio of more than 290 journals and over 2,350 books and book series volumes, as well as providing an extensive range of online products and additional customer resources and services.

Emerald is both COUNTER 4 and TRANSFER compliant. The organization is a partner of the Committee on Publication Ethics (COPE) and also works with Portico and the LOCKSS initiative for digital archive preservation.

*Related content and download information correct at time of download.

Downloaded by RMIT University At 01:30 30 June 2016 (PT)

A double-end-beam based infrared device fabricated using CMOS-MEMS process

Cheng Lei[1,2], Haiyang Mao*[2], Yudong Yang[1,2],Wen Ou[2], Chenyang Xue[1], Zong Yao[1], Anjie Ming[2] , Weibing Wang[2], Ling wang[3] , Jiandong Hu[3] and Jijun Xiong*[1]

1. Key Laboratory of Instrumentation Science & Dynamic Measurement, North University of China, Taiyuan 030051 P. R. China

2. Smart Sensing R&D Center, Institute of Microelectronics of Chinese Academy of Sciences, Beijing 100029, P. R. China

3. College of mechanical & Electrical Engineering, Henan Agricultural University，Zhengzhou 450000, P. R. China

Downloaded by RMIT University At 01:30 30 June 2016 (PT)

Abstract

Purpose –Thermopile IR detectors are one type of the most important IR devices. Considering that the surface area of conventional four-end-beam based thermopile devices cannot be effectively utilized and the performance of this type of devices is relatively low, so the paper presents a double-end-beam based thermopile device with high duty cycle and performance. The paper aims to discuss these issues.

Design/methodology/approach –Numerical analysis was conducted to show the advantages of the double-end-beam based thermopile devices.

Findings –Structural size of the double-end-beam based thermopiles may be further scaled down and maintain relatively higher responsivity and detectivity when compared with the four-end-beam based thermopiles. We characterized the thermoelectric properties of the device proposed in this paper, which achieves a responsivity of 1151.14 V/W, a detectivity of 4.15×10^8 cm Hz$^{1/2}$/W, and a response time of 14.46 ms.

Originality/value –The paper proposed a micro electro mechanical systems (MEMS) thermopile infrared sensor based on double-end-beam structure.

Keywords: thermopile; infrared sensor; double-end-beam; four-end-beam; duty cycle；numerical analysis

Paper type: Research paper

1. Introduction

Infrared (IR) sensors can detect IR radiations from both living and non-living objects, and are used in diverse applications, including night-vision equipments, spectrometry, gas analysis, temperature sensing, and imaging (Mao *et al.*, 2014; Frank and Meixner, 2001). Thermopile IR detectors based on Seebeck effect are one of the most important IR devices, as they require neither cooling systems nor alternative radiation controllers; besides, thermopile microstructures fabricated by using complementary metal-oxide-semiconductor (CMOS) technology have a significant economic advantage, making them useful as low-cost IR sensors (Xu *et al.*, 2010; Li *et al.*, 2010).

Structure of a thermopile can be classified into two kinds of structure: single layer of suspension structure and double layers of suspension structure (Xie *et al.*, 2010), according to whether thermocouple strips and absorber are typically fabricated on the same layer. Currently, the former structure is favored owing to better stability and an easier fabrication process. For the single layer of suspension structure, there are two types of structures, including closed-membrane (Wang *et al.*, 2010; Zhou *et al.*, 2013) and cantilever (Xu *et al.*, 2009; Xu *et al.*, 2010). Compared with the closed-membrane-based devices, the performance of the cantilever-based devices is relatively higher as less heat is lost in the dielectric supporting membrane. However, in cantilever-based devices, thermocouple strips are usually formed into a "cross type" structure, which is also referred to as a four-end-beam (FEB) structure (Wang *et al.*, 2010; Zhou *et al.*, 2013; Xu *et al.*, 2009; Xu *et al.*, 2010). In such a structure, the central part usually serves as an optical absorber, leaving four corners with relatively large areas wasted. That is to say, the surface area of the thermopile cannot be effectively utilized, resulting in a lower duty cycle of the device. Consequently, the performance of this type of devices is relatively low. Besides, conventional CMOS-compatible micromachined thermopiles usually adopt Xenon difluoride (XeF_2) gas to release the structures. However, such an isotropic etching step from the front-side would easily lead to excessive release, as a result, the cold junctions and the electrodes might be floated to damage.

© Emerald Group Publishing Limited
This is a pre-print of a paper and is subject to change before publication. This pre-print is made available with the understanding that it will not be reproduced or stored in a retrieval system without the permission of Emerald Group Publishing Limited.

In this paper, a MEMS thermopile-based IR sensor with high performance is presented. In the sensor, a double-end-beam (DEB) structure is adopted, and the thermocouple strips are distributed symmetrically along the longer sides of a rectangular absorber, thus facilitating the effective utilization of the surface area of the sensor. In this study, the performance of the devices with DEB structure is compared with that of conventional FEB structure to demonstrate the advantages of the former. Besides, etching-barrier structures are integrated in our device to prevent floating of cold junctions and electrodes in case of excessive release of silicon (Si) substrate beneath the beams and the absorber. Furthermore, N-type and P-type polysilicon are used as thermopile materials because of their large difference in Seebeck coefficients and small thermal conductance (Xie *et al.*, 2009). Moreover, such materials are commonly used in micro-fabrication, and the device preparation process can be fully CMOS compatible (Mao *et al.*, 2013).

2. Working principle

The thermopile is made of thermocouple strips electrically connected in series. Figure 1 shows the schematic of a basic micromachined thermopile IR detector. Thermocouple strips are supported on a floating thin dielectric layer with their hot junctions connected to the absorber area and the cold junctions located on the silicon heat-sink. Here, temperature of the heat-sink is kept consistent with the ambience. When the hot junctions are heated, temperature difference (ΔT) will be generated between the hot junctions and the cold junctions. According to Seebeck effect, a thermoelectric output voltage (ΔU) can be generated at the cold junctions, without applying any bias voltage to the strips. The ΔU of the thermopile can be calculated using the following expression

$$\Delta U = N\alpha\Delta T \quad (1)$$

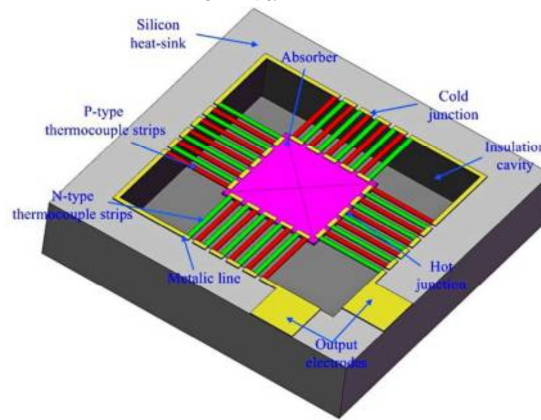

Figure 1. Schematic of a basic micromachined thermopile IR detector

where N is the number of thermocouple strips, α is the difference between the Seebeck coefficients (μV/K) of the two thermoelectric materials. The responsivity (V/W) of the device can be obtained as follows (Escriba *et al.*, 2005)

$$R_v = \frac{\Delta U}{P_0} = \frac{\Delta U}{\varphi_0 A_d} = \frac{N \cdot \alpha \cdot \eta}{G_{th}}, \quad (2)$$

where P_0 is the radiation power, φ_0 is the power density of the IR radiation, A_d is the area of the absorber, η is the absorption rate of the absorber, and G_{th} is the entire thermal conductance of the thermopile that consists of three parts: thermal conductance of the structure G_s, thermal conductance of the atmospheric air G_g, and thermal conductance of the radiation G_r. Therefore, the entire thermal conductance of the thermopile can be calculated by

$$G_{th} = G_s + G_g + G_r \quad (3)$$

Thermal conductance of the atmospheric gas and radiation are usually negligible when the device operates in vacuum and at low temperature (Sun *et al.*, 2013). Therefore, the entire thermal conductance of the thermopile can be also written as

$$G_{th} = G_s \quad (4)$$

where G_s can be expressed as (Du *et al.*, 2002)

$$G_s = \sum_{i=1}^{4} N \frac{\lambda_i \cdot d_i \cdot w_i}{l_i}. \quad (5)$$

Herein, λ_i, w_i, d_i, and l_i, respectively, are the thermal conductivity, width, thickness, and length of each thermocouple strip (i = 1 for the P-type thermocouple strips; i = 2 for the N-type thermocouple strips; i = 3 for the isolation layer; i = 4 for the supporting membrane). Further, the responsivity of the device can be calculated by using the expression

Downloaded by RMIT University At 01:30 30 June 2016 (PT)

© Emerald Group Publishing Limited
This is a pre-print of a paper and is subject to change before publication. This pre-print is made available with the understanding that it will not be reproduced or stored in a retrieval system without the permission of Emerald Group Publishing Limited.

$$R_{\rm v} = \frac{\eta \cdot \alpha}{\sum_{i=1}^{4} \frac{\lambda_{\rm i} \cdot d_{\rm i} \cdot w_{\rm i}}{l_{\rm i}}} . \tag{6}$$

The detectivity can be calculated as

$$D^{*} = R_{\rm v}\sqrt{\frac{A_{\rm d}}{4kT_0R_0}} , \tag{7}$$

where k is the Boltzmann constant, and R_0 is the electric resistance of the thermopile strips. The electric resistance of the thermopile strips can be calculated as (Escriba *et al.*, 2005)

$$R_0 = N\sum_{i=1}^{2}\gamma_{\rm i}\frac{l_{\rm i}}{d_{\rm i} \cdot w_{\rm i}} , \tag{8}$$

where $\gamma_{\rm i}$ is the resistivity of the thermocouple strips. Another important parameter is the response time (τ), which can be expressed as

$$\tau = \frac{C_{\rm th}}{G_{\rm th}} , \tag{9}$$

where $C_{\rm th}$ is the entire thermal capacitance of the thermopile. We can also calculate $C_{\rm th}$ as

$$C_{\rm th} = \sum_{\rm i=1}^{4}\left[l_{\rm i} \cdot w_{\rm i} \cdot d_{\rm i} \cdot \rho_{\rm i} \cdot c_{\rm i}\right] + \sum_{\rm j=5}^{7}\left[A_{\rm d} \cdot d_{\rm j} \cdot \rho_{\rm j} \cdot c_{\rm j}\right] , \tag{10}$$

Where $\rho_{\rm i}$ and $c_{\rm i}$ are the mass density and the specific heat of each thermocouple strip; $d_{\rm j}$, $\rho_{\rm j}$, and $c_{\rm j}$, respectively, are the thickness, mass density, and specific heat of each part of the absorber ((j = 5 for the absorber; j = 6 for the supporting membrane of the absorber; j = 7 for the isolation layer of the absorber).

We have $l_{\rm i}=L$, where L stands for the equivalent length of each part of the thermocouple zone. Substituting $l_{\rm i}=L$ into Eq. (6), we can write the expression for the responsivity of the device as

$$R_{\rm v} = \left(\frac{\eta \cdot \alpha}{\sum_{i=1}^{4}\lambda_{\rm i} \cdot d_{\rm i} \cdot w_{\rm i}}\right) \cdot L . \tag{11}$$

Substituting Eqs. (8), and (11) into Eq. (7), the detectivity can be written as

$$D^{*} = \left(\frac{\eta\alpha}{\sqrt{4kT_0}} \cdot \frac{\frac{1}{\sum_{i=1}^{4}\lambda_{\rm i} \cdot d_{\rm i} \cdot w_{\rm i}}}{\sqrt{\left(\sum_{i=1}^{2}\gamma_{\rm i}\frac{1}{d_{\rm i} \cdot w_{\rm i}}\right)}} \cdot \frac{1}{\sqrt{N}}\right) \cdot \sqrt{A_{\rm d} \cdot L} , \tag{12}$$

Substituting Eqs. (4), (5), and (10) into Eq. (9), the expression for the response time can be written as

$$\tau = \left(\frac{1}{N} \cdot \frac{1}{\sum_{i=1}^{4}\lambda_{\rm i} \cdot d_{\rm i} \cdot w_{\rm i}}\right)\left\{L^2\sum_{\rm i=1}^{4}\left[w_{\rm i} \cdot d_{\rm i} \cdot \rho_{\rm i} \cdot c_{\rm i}\right] + (A_{\rm d} \cdot L) \cdot \sum_{\rm j=5}^{7}\left[d_{\rm j} \cdot \rho_{\rm j} \cdot c_{\rm j}\right]\right\} . \tag{13}$$

3. Structural design

In order to further improve the performances of the thermopile devices, a thermopile based on the DEB structure is presented. Thermo-electric properties of various materials used in thermopile design are listed in Table 1. Here, Al, SiO_2, and SiN_x are abbreviations of aluminum, silicon dioxide, and silicon nitride, respectively. Figure 2 schematically displays a conventional FEB structure (Figure 2(a)) and the proposed DEB structure (Figure 2(b)). As illustrated in Figure 2(a), the thermocouple strips are distributed symmetrically along the sides of the square-shaped absorber. The hot junctions overlap the absorber and the cold junctions overlap the heat sink. The N-type and P-type polysilicon thermocouple strips are located on two different layers and are all connected in series by aluminum lines to form the thermopile. $W_{\rm a1}$ and L_1 stand for the width of the absorber and the length of the thermocouple strips, respectively. In the DEB-based device (Figure 2 (b)), the absorber is rectangular in shape. The thermocouple strips are distributed symmetrically along the longer sides of the rectangular absorber. $L_{\rm a2}$ and $W_{\rm a2}$ are the length and width of the absorber, respectively. L_2 stands for the length of the thermocouple strips. Compared with the FEB-based devices, the DEB-based ones effectively utilize the surface area located at four corners of the device, so as to increase the absorber area and reduce the thermal conductance of the structure. As a result, the FEB-based devices exhibit higher responsivity and detectivity, and the following numerical analysis shows the advantages of the DEB-based devices.

Downloaded by RMIT University At 01:30 30 June 2016 (PT)

© Emerald Group Publishing Limited
This is a pre-print of a paper and is subject to change before publication. This pre-print is made available with the understanding that it will not be reproduced or stored in a retrieval system without the permission of Emerald Group Publishing Limited.

Downloaded by RMIT University At 01:30 30 June 2016 (PT)

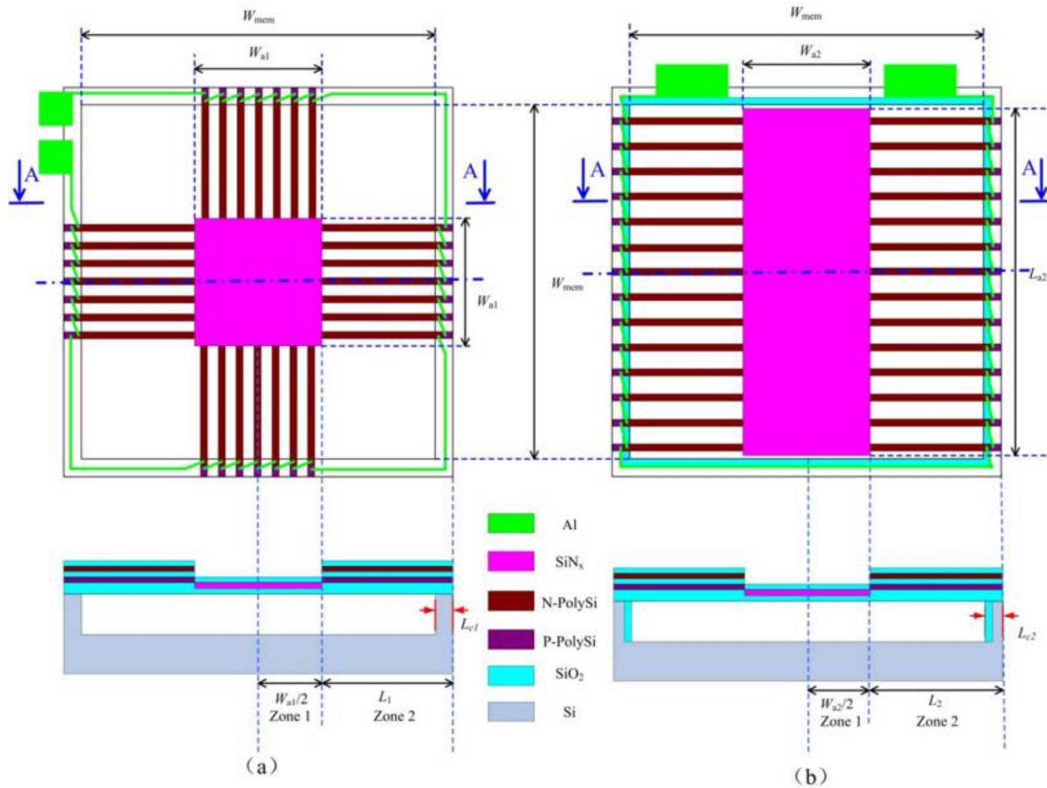

Figure 2. Surface and cross-section diagrams of (a) a FEB thermopile, and (b) a DEB thermopile

Table 1. Thermo-electric properties of various materials used in thermopile design.
(Allison *et al.*, 2003; McConnell *et al.*, 2001; Strasser *et al.*, 2004)

Materials	Al	N-type polysilicon (doped @ 3.64E20 cm^{-3})	P-type polysilicon (doped @ 1.82E20 cm^{-3})	SiO_2	SiN_x
Seebeck coefficient (μVK^{-1})	– 1.66	– 124.17	105.76	—	—
Thermal conductivity (Wm^{-1}K^{-1})	237	35	30	1.2	16.7
Resistivity (μΩ m)	0.03	2.7	6.55	—	—

As parameters such as width (w_i), thickness (d_i, d_j), thermal conductivity (λ_i), mass density (ρ_i, ρ_j), specific heat (c_i, c_j) of the two types of devices in design may achieve equal values through the same microfabrication process flow, we take into consideration only the influence of the area of absorber and the length of thermocouple strips. Hence, the expressions for responsivity, detectivity, and response time can be written as

$$R_{vk} = (\eta\alpha B_0)\cdot L_k \tag{14}$$

$$D_k^* = (\frac{\eta\alpha}{\sqrt{4kT_0}}\cdot\frac{1}{\sqrt{N_0}}\cdot\frac{B_0}{\sqrt{C_0}}\cdot)\sqrt{A_{dk}\cdot L_k} \tag{15}$$

$$\tau_k = \frac{B_0\cdot D_0}{N_0}\cdot L_k^{\ 2} + \frac{B_0\cdot E_0}{N_0}\cdot A_{dk}\cdot L_k \tag{16}$$

where $B_0 = \frac{1}{\sum_{i=1}^{4}\lambda_i\cdot d_i\cdot w_i}$, $C_0 = \sum_{i=1}^{2}\gamma_i\frac{1}{d_i\cdot w_i}$, $D_0 = \sum_{i=1}^{4}\left[w_i\cdot d_i\cdot\rho_i\cdot c_i\right]$, $E_0 = \sum_{j=5}^{7}\left[d_j\cdot\rho_j\cdot c_j\right]$, $N_0 = N$. Here, R_{vk}, D_k^*, τ_k, L_k, and A_{dk} are the responsivity, detectivity, response time, length of thermocouple strips, and area of the absorber (k = 1 for the FEB structure and k = 2 for the DEB structure). Meanwhile, both structures are divided into two zones (Xu *et al.*, 2010), namely, Zone 1 and Zone 2. Herein, Zone 1 refers to the absorber part, and Zone 2 refers to the thermopile region.

© Emerald Group Publishing Limited
This is a pre-print of a paper and is subject to change before publication. This pre-print is made available with the understanding that it will not be reproduced or stored in a retrieval system without the permission of Emerald Group Publishing Limited.

Besides, both of these two structures have an insulation cavity with the same dimension, which is $W_{mem} \times W_{mem}$. Herein, W_{mem} can be described as

$$W_{mem} = W_{a1} + 2 \cdot L_1 - L_{c1}, \tag{17}$$

$$W_{mem} = W_{a2} + 2 \cdot L_2 - L_{c2}, \tag{18}$$

where L_{c1} and L_{c2} are the lengths of the cold junctions for the two structures, respectively. The lengths of the cold junctions are considerably shorter than that of the thermocouple strips. In addition, the aluminum lines located at positions of the cold junctions are very close to the edges of the opening above the heat insulation cavity, that is to say, L_{c1} and L_{c2} are very small, which can be negligible. Only in this way, while the device is working, the thermoelectric response current would scarcely pass through the cold junctions. Consequently, we can get

$$W_{mem} \approx W_{a1} + 2 \cdot L_1, \tag{19}$$

$$W_{mem} \approx W_{a2} + 2 \cdot L_2. \tag{20}$$

Therefore, we have

$$W_{a1} = W_{mem} - 2 \cdot L_1, \tag{21}$$

$$W_{a2} = W_{mem} - 2 \cdot L_2. \tag{22}$$

In order to obtain devices with high performance, the absorber area is usually set at a value which is large enough, but not larger than the size of its insulation cavity. That is to say, $L_{a2} \approx W_{mem}$, but $L_{a2} < W_{mem}$. Hence, we assume

$$L_{a2} = W_{mem}. \tag{23}$$

The area of the absorber (A_{dk}) can be written as functions of the length (L_k) of the thermocouple strips. Thus A_{d1} and A_{d2} are written respectively as

$$A_{d1} = W_{a1}{}^2 = (W_{mem} - 2L_1)^2 \tag{24}$$

$$A_{d2} = L_{a2} \times W_{a2} = W_{mem} \times (W_{mem} - 2L_2) \tag{25}$$

Relationship between the area of absorber (A_{d1} and A_{d2}) and the length of the thermocouple strips (L_k) is shown in Figure 3. When the FBE-based device adopts a random point $\psi_1(a_1, b_1)$ in curve A_{d1} to design A_{d1} and L_1, as long as the DBE-based devices adopt a random point in curve A_{d2} between point $\psi_2(a_1, b_2)$ and point $\psi_3(a_2, b_1)$ to design A_{d2} and L_2, both the strip length and the absorber area for DBE-based devices will be much larger than that of the FBE-based device. In other words, according to Eqs. (14) and (15), the responsivity and detectivity of DBE-based devices will be higher than that of FEB-based devices. Therefore the DEB structure was adopted in our work so as to obtain higher responsivity and the detectivity of the device. As should be noted, although the DBE thermopile has advantages with regard to responsivity and detectivity, accordingly to Eq. (16), there is still a drawback with respect to response time that will increase. Besides, according to Eq. (14) and (15), structural size of the DEB-based thermopiles may be further scaled down by reducing the length of the absorber (at the expense of reducing A_{d2}), and maintain relatively higher responsivity and detectivity by reducing the number of thermocouple strips (N_0) when compared with the FEB-based one.

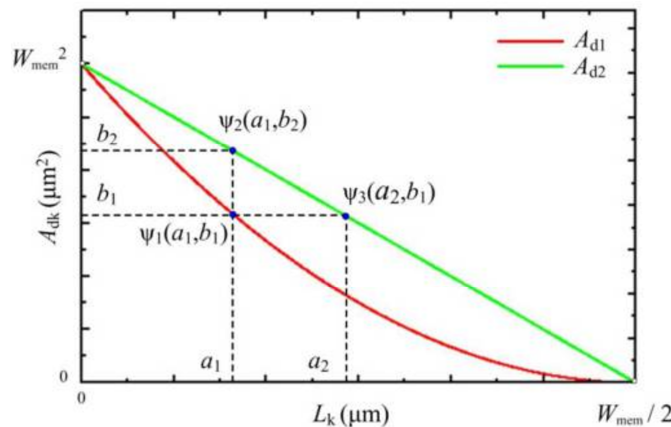

Figure 3 Relationship between the area of absorber and the length of thermocouple strips

Table 2 lists the structural parameters of DEB-based thermopile device in this work and FEB-based thermopile

Downloaded by RMIT University At 01:30 30 June 2016 (PT)

© Emerald Group Publishing Limited
This is a pre-print of a paper and is subject to change before publication. This pre-print is made available with the understanding that it will not be reproduced or stored in a retrieval system without the permission of Emerald Group Publishing Limited.

device in previous research. Based on these parameters, performance parameters of the device are theoretically calculated. Table 3 lists theoretical values of performance parameters in both thermopile devices.

Table 2. Parameters of the thermopile devices presented in this work and previous research

	Double-end-beam thermopile device	Four-end-beam thermopile device
N-type polysilicon (L × W × H)	183 × 5 × 0.55 μm^3	130 × 5 × 0.55 μm^3
P-type polysilicon (L × W × H)	198 × 5 × 0.55 μm^3	145× 5 × 0.55 μm^3
SiO_2 electric isolation layer (H)	0.4 μm	0.4 μm
Absorber area (L × W)	500 × 200 μm^2	310× 310 μm^2
Insulation cavity (L × W)	570× 540 μm^2	570× 570 μm^2
The number of thermocouple strips	96	116

Table 3. Theoretical values of performance parameters of the devices presented in this work and previous research

	Double-end-beam thermopile device	Four-end-beam thermopile device
R_v (V/W)	255.83	148.89
D^* (cm $Hz^{1/2}$/W)	2.54×10^8	1.52×10^8
τ (ms)	13.09	7.10

4. Fabrication

Figure 4 shows the CMOS-compatible microfabrication process flow of the DEB thermopiles reported in this paper. The starting wafer was a single-side polished 6-inch p-type silicon wafer with <100> orientation and 675 μm thickness.

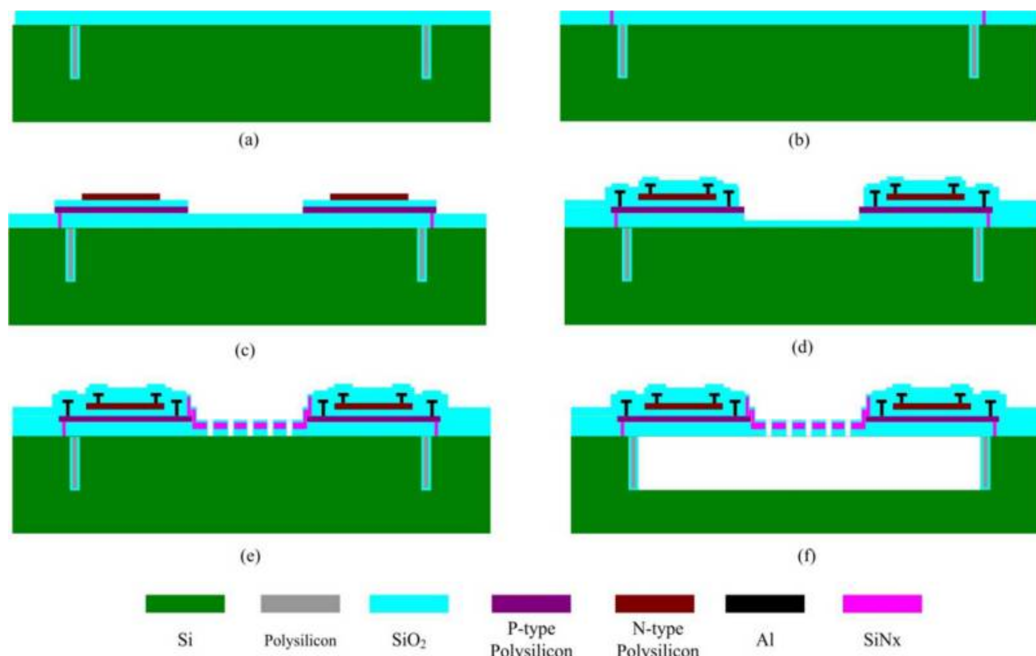

Figure 4. Fabrication process of the thermopile device

In order to realize etching-barrier structures, at beginning of the process, a ring-shaped deep trench with a depth of approximately 30 μm was formed by using deep reactive-ion etching (DRIE). Then, the trench was filled with thermal SiO_2 and polysilicon deposited by using a low pressure chemical vapor deposition (LPCVD) process. After reversed etching of the thermal SiO_2 and the polysilicon layers, an 8000 Å thermal SiO_2 layer was deposited onto the wafer as the electric isolation and mechanical supporting layer (Shown in Figure 4 (a)).

After that, windows were opened in the SiO_2 layer at the cold junctions of thermopiles, and a SiN_x layer was deposited and photo-patterned to fill the windows as demonstrated in Figure 4 (b). In this way, heat sinks were formed. With these heat sinks, the temperature of the cold junctions and the Si substrate could be kept the same.

Subsequently, three layers of films, which were 5500 Å polysilicon, 4000 Å SiO_2 and 5500 Å polysilicon, were deposited alternatively by using the LPCVD process (Shown in Figure 4 (c)). Herein, the two polysilicon layers were P-type and N-type doped. The P-type polysilicon located at the lower layer was implanted with B^+, using a doping dose

Downloaded by RMIT University At 01:30 30 June 2016 (PT)

© Emerald Group Publishing Limited
This is a pre-print of a paper and is subject to change before publication. This pre-print is made available with the understanding that it will not be reproduced or stored in a retrieval system without the permission of Emerald Group Publishing Limited.

of 10^{16} cm^{-2} and an implantation energy of 65 keV. Similarly, the N-type polysilicon was implanted with P^- of 2×10^{16} cm^{-2} @ 80 keV. The SiO_2 layer between the two polysilicon films serves as an electric insulator. Later on, the three layers were photo-patterned to form thermocouple strips.

The thermocouple strips were covered by a 4000 Å SiO_2 layer, which was formed by plasma enhanced chemical vapor deposition (PECVD) and was used as the first passivation layer in the structure. Then, contact holes were opened by a reactive ion etching (RIE) step. After that, Al was sputtered and patterned on the passivation layer to realize electric connections among the thermocouple strips. Next, another passivation layer (4000 Å SiO_2 formed by PECVD) was deposited over the Al lines. Subsequently, the SiO_2 layer over the P-type strips at the ends of the hot junctions was removed, revealing part of the P-type strips (Figure 4 (d)).

A 6000 Å SiN_x film was deposited and patterned into the absorber. The SiNx at the absorber edges covers the revealed hot junction ends of the P-type strips, thus reducing the heat loss at the hot junctions. Further, a SiO_2 dielectric layer was deposited by PECVD, and then releasing windows were opened within the absorber region (Figure 4 (e)). The wafer was isotropically etched by XeF_2 gas to remove the silicon substrate beneath the thermopile structure (Figure 4 (f)). After XeF_2 dry etching, a cavity under the membrane was formed for thermal isolation. The fabricated DEB-based thermopile devices in this work and FEB-based one in previous research are shown in Figure 5. An SEM image of the structure of FEB-based device is shown in figure 5(a), the structure of DEB-based device is shown in figure 5(b), and that of the cross section and the cold and hot-junction areas are shown in Fig. 5 (c)-(e).

Downloaded by RMIT University At 01:30 30 June 2016 (PT)

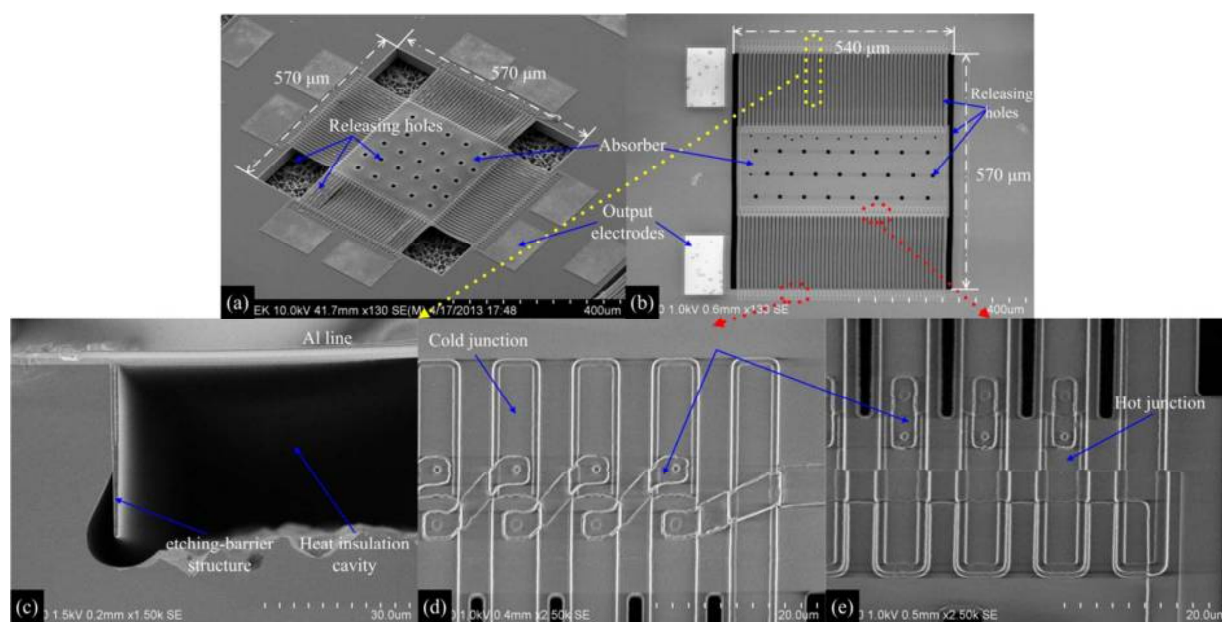

Figure 5. SEM images of (a) the structure of FEB-based device, (b) the structure of DEB-based one, and that of (c) the cross-section and (d) the cold-junction and (e) the hot-junction areas

5. Measurement and discussion

In order to characterize the properties of the detectors, a measurement system shown in Figure 6 was set up. During the measurement, the detector was installed within a cooling system, which was used to consistently maintain the temperature of the heat sink with respect to the ambient temperature (22 °C @ 36% RH). The cooling system was placed in front of the blackbody, and the distance between the blackbody and the detector was fixed at 9 cm. The temperature of the blackbody was set at 500 K for detector characterization. Herein, the applied IR power density on the detector surface was 66.72 W/m^2. Besides, in this system, a mechanical chopper was used to control the chopping frequency, and a low-pass filter circuit module was devoted to avoiding the effect of high-frequency noise. A semiconductor parameter analyzer was utilized to output the signals. The I-V curve of the detector is presented in Figure 7, according to which, the electric resistance R_0 of the thermopile strips is 458.5 kΩ. For a chopping frequency of 4 Hz, several cycles of output voltage waveform is illustrated in Figure 8 (a), in which a 7.47 mV signal difference can be observed. The response time obtained by magnifying a rising edge of the signal in one of the cycles is 14.46 m s (shown in Figure 8 (b)).

© Emerald Group Publishing Limited
This is a pre-print of a paper and is subject to change before publication. This pre-print is made available with the understanding that it will not be reproduced or stored in a retrieval system without the permission of Emerald Group Publishing Limited.

Downloaded by RMIT University At 01:30 30 June 2016 (PT)

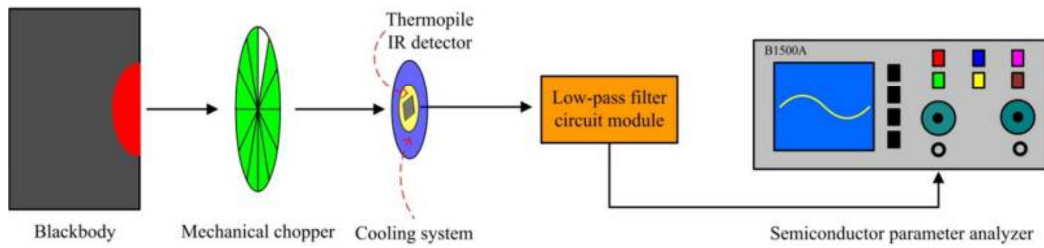

Figure 6. Schematic of measurement system for IR radiation characterization

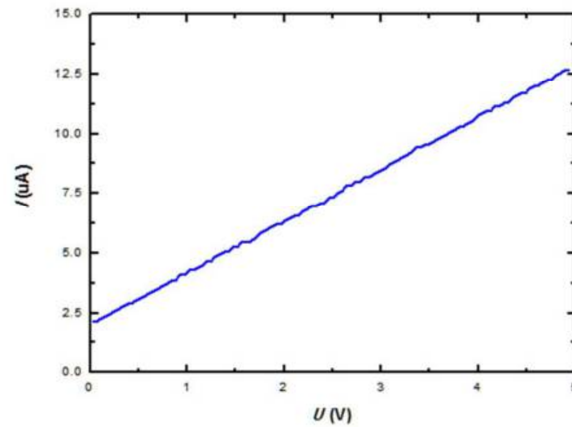

Figure 7. Measured I-V curve for the detectors

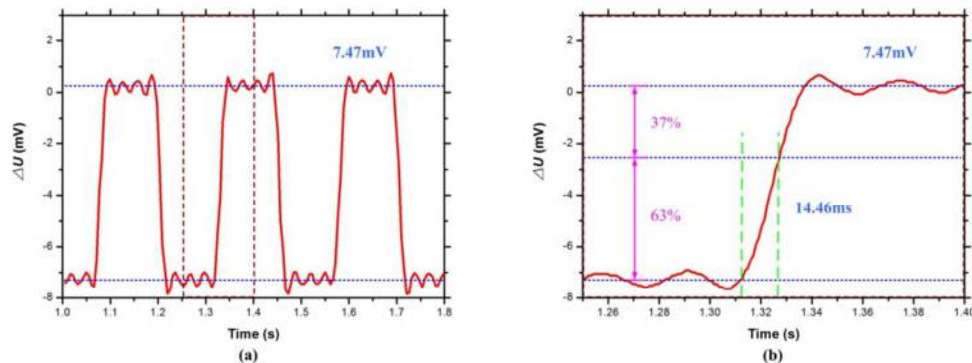

Figure 8. Output signals (a) with several cycles and (b) within a rising edge of the DEB-based thermopile device at 4 Hz and 500K

Based on the theories discussed in Section 2, performance parameters of the IR thermopile detector can be calculated. The responsivity R_v calculated from the response voltage amplitude by using Eq. (2) is 1151.14 V/W. Similarly, the detectivity D^* reaches 4.15×10^8 cm $Hz^{1/2}$/W according to Eq. (7). Similarly, measured values of performance parameters of the FEB-based thermopiles in previous research were obtained. Table 4 lists measured values of performance parameters of both devices. As shown table 1, the DEB-based thermopile device has responsivity ~75% larger and detectivity ~73% larger than that of the FEB-based one. The values of R_v and D^* obtained are relatively larger than the theoretically calculated ones due to overvalued doping concentrations in the implantation processes. In practical implantation, the actual projected ranges might reach a distance beyond the central line of the polysilicon layers; therefore, the doping concentrations might be smaller than the theoretical values. Thus the Seebeck coefficients are enhanced (Strasser *et al.,* 2004), and at the same time, the electric resistance R_0 is also increased. Because of the growth in R_0, the extent of increasment in D^* could not be as high as that in R_v.

© Emerald Group Publishing Limited
This is a pre-print of a paper and is subject to change before publication. This pre-print is made available with the understanding that it will not be reproduced or stored in a retrieval system without the permission of Emerald Group Publishing Limited.

Table 4. Measured values of performance parameters of both device

	DEB-based thermopile device	FEB-based thermopile device
R_0 (kΩ)	458.5	434
ΔU (V)	7.34	4.09
R_v (V/W)	1151.14	656.23
D^* (cm $Hz^{1/2}$/W)	4.15×10^8	2.41×10^8
τ (ms)	14.46	11.70

6. Conclusions

In this work, a DEB-based IR device was designed and fabricated using a CMOS-compatible process. Theoretical analysis suggests that structure size of the DEB-based device may be further scaled down and has advantages over the FEB device in aspects of responsivity and detectivity. Preliminary measurement results demonstrated that the DEB-based IR device presented in our work has responsivity ~75% larger and detectivity ~73% larger than that of the FEB-based one in previous research, and achieves a responsivity of 1151.15 V/W, a detectivity of 4.15×10^8 cm $Hz^{1/2}$/W, and a response time of 14.46 ms. Meanwhile, an etching-barrier structure is adopted to prevent floating of cold junctions and electrodes in case of excessive etching of the heat insulation cavity, as a result, product yield of the devices may be further improved. Such an IR device might have wide applications on gas analysis, temperature measuring, thermoelectric converter and so on.

Downloaded by RMIT University At 01:30 30 June 2016 (PT)

Acknowledgement

This work was supported by National Natural Science Foundation of China (Grant No. 61401458, 61335008, 61136006 & 51205373), Jiangsu Natural Science Foundation (Grant No. BK20131098), and Henan Province Collaborative Projects in Science and Technology (132106000073).

REFERENCES

Mao, H., Lei, C., Chen, Y., Chen, Z., Ou, W., Wu, W., Ming, A., and Chen D. (2014), "Nanofiber forests with high infrared absorptance**",** *In Proceedings of the 27th IEEE International Conference on Micro Electro Mechanical Systems*, San Francisco, CA, USA, 26 - 30 January 2014; pp. 644-647.

Frank, J., and Meixner, H. (2001), "Sensor system for indoor air Monitoring using semiconducting metal oxides and IR-absorption", *Sens. Actuator B Chem.*, Vol. 78 No. 1-3, pp. 298-302

Xu, D., Xiong, B., and Wang, Y. L. (2010), "A CMOS compatible micromachined thermopile IR sensor with high sensitivity", *Electrochem. Solid-State Lett.*, Vol. 13 No. 9, pp. J106-J109

Li, Y., Zhou, H., Li, T., Wang, Y., Liu, Y., and Wang, Y. (2010), "CMOS-compatible 8×2 thermopile array", *Sens. Actuator A Phys*., Vol. 161 No. 1-2, pp. 120-126

Xie, J., Lee, C., and Feng, H. (2010), "Fabrication, and Characterization of CMOS MEMS-Based Thermoelectric Power Generators", *J. Microelectromech. Syst.*, Vol. 19 No. 2, pp. 317-324

Wang, K., Xue, C., Liang, T., Jiao, B., Zhang, W., Chen, D., and Xiong, J. (2010), "Thermopile infrared detector with detectivity greater than 10^8 cm $Hz^{(1/2)}$/W", *J. Infrared Milli. W.*, Vol. 31 No. 7, pp. 810-820

Zhou, H., Kropelnicki, P., Tsai, J. M., and Lee, C. (2013), "Development of a thermopile infrared sensor using stacked double polycrystalline silicon layers based on the CMOS process", *J. Micromech. Microeng.*, Vol. 23 No. 6, pp. 1-14

Xu, D., Xiong, B., Wang, Y., Liu, M., and Li, T. (2009), "Integrated micromachined thermopile IR detectors with an XeF_2 dry-etching process", *J. Micromech. Microeng.*, Vol. 19 No. 12, pp. 1-11

Xie, J., Lee, C., Wang, M. F., Liu, Y., and Feng, H. (2009), "Characterization of heavily doped polysilicon films for CMOS-MEMS thermoelectric power generators", *J. Micromech. Microeng.*, Vol. 19 No. 12, pp. 1-8

Mao, H., Chen, Y., Ou, Y., Ou, W., Xiong, J., You, C., Tan, Q. and Chen, D. (2013), " Fabrication of nanopillar forests with high infrared absorptance based on rough poly-Si and spacer technology", *J. Micromech. Microeng.*, Vol. 23 No. 9, pp. 1-6

Escriba, C., Campo, E., Esteve, D., and Fourniols, J. Y. (2005), " Complete analytical modeling and analysis of

© Emerald Group Publishing Limited
This is a pre-print of a paper and is subject to change before publication. This pre-print is made available with the understanding that it will not be reproduced or stored in a retrieval system without the permission of Emerald Group Publishing Limited.

micromachined thermoelectric uncooled IR sensors", *Sens. Actuator A Phys.*, Vol. 120 No. 1, pp. 267-276

Sun, X., Xu, D., Xiong, B., Wu, G., and Wang, Y. (2013), "A wide measurement pressure range CMOS-MEMS based integrated thermopile vacuum gauge with an XeF2 dry-etching process", *Sens. Actuator A Phys.*, Vol. 201 No. 12, pp. 428-433

Du, C. H., and Lee, C. (2002), "Characterization of thermopile based on complementary metal-oxide semiconductor materials and post CMOS micromachining", *JPN. J. Appl. Phys.*, Vol. 41 No. 6S, pp. 4340-4345

Allison, S. C., Smith, R. L., Howard, D. W., Gonzalez, C., and Collins, S. D. (2003), "A bulk micromachined silicon thermopile with high sensitivity", *Sens. Actuator A Phys.*, Vol. 104 No. 1, pp. 32-39

McConnell, A. D., Uma, S., and Goodson, K. E. (2001), "Thermal Conductivity of doped polysilicon layers", *J. Microelectromech. Syst.*, Vol. 10 No. 3, pp. 360-369

Strasser, M., Aigner, R., Lauterbach, C., Sturm, T. F., Franosch, M., and Wachutka, G. (2004), "Micromachined CMOS thermoelectric generators as on-chip power supply", *Sens. Actuator A Phys.*, Vol. 114 No. 2, pp. 362-370

Xu, D., Xiong, B., and Wang, Y. (2010), "Modeling of front-etched micromachined thermopile IR detector by CMOS technology", *J. Microelectromech. Syst.*, Vol. 19 No. 6, pp. 1331-1340

Corresponding Author:

*Haiyang Mao E-mail: maohaiyang@ime.ac.cn, Tel.: +86-10-82995932, Fax: 86-10-82995932

*Jijun Xiong E-mail: xiongjijun@nuc.edu.cn, Tel.: +86-351-3924891, Fax: +86-351-3922131

Downloaded by RMIT University At 01:30 30 June 2016 (PT)

© Emerald Group Publishing Limited
This is a pre-print of a paper and is subject to change before publication. This pre-print is made available with the understanding that it will not be reproduced or stored in a retrieval system without the permission of Emerald Group Publishing Limited.